Biophysical *Journal*
Article

Biophysical Society

Lipid Configurations from Molecular Dynamics Simulations

Weria Pezeshkian,[1] Himanshu Khandelia,[1] and Derek Marsh[1,2,*]
[1]MEMPHYS-Centre for Biomembrane Physics, University of Southern Denmark, Odense M, Denmark and [2]Max-Planck-Institut für biophysikalische Chemie, Göttingen, Germany

ABSTRACT The extent to which current force fields faithfully reproduce conformational properties of lipids in bilayer membranes, and whether these reflect the structural principles established for phospholipids in bilayer crystals, are central to biomembrane simulations. We determine the distribution of dihedral angles in palmitoyl-oleoyl phosphatidylcholine from molecular dynamics simulations of hydrated fluid bilayer membranes. We compare results from the widely used lipid force field of Berger et al. with those from the most recent C36 release of the CHARMM force field for lipids. Only the CHARMM force field produces the chain inequivalence with *sn*-1 as leading chain that is characteristic of glycerolipid packing in fluid bilayers. The exposure and high partial charge of the backbone carbonyls in Berger lipids leads to artifactual binding of Na^+ ions reported in the literature. Both force fields predict coupled, near-symmetrical distributions of headgroup dihedral angles, which is compatible with models of interconverting mirror-image conformations used originally to interpret NMR order parameters. The Berger force field produces rotamer populations that correspond to the headgroup conformation found in a phosphatidylcholine lipid bilayer crystal, whereas CHARMM36 rotamer populations are closer to the more relaxed crystal conformations of phosphatidylethanolamine and glycerophosphocholine. CHARMM36 alone predicts the correct relative signs of the time-average headgroup order parameters, and reasonably reproduces the full range of NMR data from the phosphate diester to the choline methyls. There is strong motivation to seek further experimental criteria for verifying predicted conformational distributions in the choline headgroup, including the ^{31}P chemical shift anisotropy and ^{14}N and CD_3 NMR quadrupole splittings.

INTRODUCTION

General principles governing lipid conformations in bilayer membranes have been established from x-ray crystal structures for a range of different phospholipids, glycolipids, diglycerides, and ceramides (1–4). The bilayer crystal structure of glycerolipids is characterized by the backbone dihedrals, and by which of the *sn*-1 and *sn*-2 chains is the leading one, i.e., the one which proceeds directly into the bilayer from attachment to the glycerol. To achieve parallel chain packing, the other chain is then bent by 90°. The polar headgroup structure is bent down, parallel to the bilayer plane, and is characterized by a limited number of conformations in the case of phosphatidylcholine, or, for phosphatidylethanolamine, by just two mirror-image conformers.

In contrast, some of the crystal structures of lipids associated with both soluble and membrane proteins that are deposited in the Protein Data Bank (PDB) violate several of the conformational principles derived from small-molecule x-ray methods (5–7). This includes incorrect stereochemistry. Much of the chain configurational disorder arises from energetically disallowed *skew* conformations. Eclipsed conformations occur in some glycerol backbone torsion angles and in C−C torsion angles of the lipid headgroups. A high proportion of the carboxyl ester groups are in nonplanar configurations, and certain of the carboxyls are in the disallowed *cis* configuration. Some structures have the incorrect enantiomeric configuration of the glycerol backbone, and many branched methyl groups in the phytanyl chains of archaeal lipids are in the incorrect *S*-configuration. Whatever the dynamic state of the lipids, these incorrect structures cannot describe lipid-protein interactions in biological membranes.

Experimental data on the dynamic lipid structures that occur in fluid bilayer membranes come mostly from magnetic resonance studies. Universally, the *sn*-1 and *sn*-2 acyl chains are inequivalent in fluid bilayers, with *sn*-1 as the leading chain (8–10). In particular, ^2H-NMR studies suggest that the headgroup structures can be explained minimally by exchange between two mirror conformations

Submitted August 11, 2017, and accepted for publication February 13, 2018.

*Correspondence: dmarsh@gwdg.de

Editor: Markus Deserno.
https://doi.org/10.1016/j.bpj.2018.02.016

(11,12). Correspondingly, liquid-state NMR of phospholipid micelles is interpreted in terms of exchange between stable conformers of the glycerol backbone (1). A single consensus structure was proposed that is consistent with a considerable range of different solid-state NMR couplings for phosphatidylcholine bilayers (13). However, this incorporates a conformationally forbidden nonplanar ester carboxyl and a relatively high-energy glycerol backbone configuration. This, therefore, also suggests the presence of a limited number of interconverting conformers.

Molecular dynamics (MD) simulations, in principle, are capable of yielding the dynamic configurations of lipid molecules assembled in bilayer membranes, and at a level of atomic detail that is not available directly from spectroscopic studies. However, we can expect these time-averaged configurations to depend more or less sensitively on the force fields chosen for the simulations (14–16). In general, force fields are optimized to reproduce a range of experimental parameters that characterize the ensemble bilayer structure (17,18). It is therefore of direct relevance to inquire how this impacts the molecular configurations of the constituent lipids. Specifically, correct conformational structures are needed for a realistic and effective description of intermolecular interactions, for example, in lipid-protein interactions, and in lipid-cholesterol interactions that give rise to formation of liquid-ordered membrane domains (i.e., rafts).

Here, we determine dihedral-angle distributions for a representative membrane phospholipid, 1-palmitoyl-2-oleoyl-*sn*-glycero-3-phosphocholine (POPC), in fully hydrated bilayers. These are equilibrated in MD simulations under the action of two different widely used phospholipid force fields. We compare the earlier united-atom model of Berger et al. (19,20) with the most recent version of the CHARMM 36 all-atom force field for lipids (21). The natural equilibrium state of a flat bilayer membrane is one that is essentially free of tension, even when undulations are taken into account (22,23). Although the force field of Berger et al., with Lennard-Jones potential adjusted to experimental results for pentadecane and headgroup partial charges of Chiu et al. (24), produces fluid-phase packing for tension-free bilayers above the chain-melting temperature, this was not the case until the C36 release of the CHARMM force field, for *NPT* ensembles (17). A significant feature of the nonbonded interactions is the partial charge on the carboxyl ester groups (18), which, besides affecting lipid packing, can exaggerate the degree of monovalent cation binding (25–27). Thus, we might expect this also to affect the configuration of the glycerolipid backbone and attached chains.

The motivation behind this study is twofold: to assess the extent to which the MD structures from the different force fields conform to the configurational principles established from crystal structures and time-average NMR order parameters, and to identify structural features that might be used for future validation. Force field development is a continual process (17), and there is a constant need for further targets with which to test them (28). A previous survey of lipid force fields concludes the need for improved agreement with NMR data on the glycerol backbone and choline headgroup (29). We strengthen this here with consideration of ^{31}P-NMR chemical shift anisotropy and ^{14}N-NMR quadrupole splittings. Furthermore, we find that headgroup orientations (i.e., order parameters) may be interpreted realistically in terms of rapid exchange between the principal crystalline conformers. This analytic strategy has been challenged as oversimplifying but never specifically tested. The possibility to describe the dynamic structure of fluid lipid bilayers in terms of a limited number of molecular configurations then gives us a conceptual framework for understanding and interpreting the properties of biological membranes, which are at the same time both highly dynamic and highly ordered.

These results should be of wide interest to workers in the field of lipid membranes (i.e., all biological membranes), as well as to all those wishing to appreciate both the implications and limitations of MD simulations in biological systems. Ever since the first crystal structure of a phospholipid was determined, conformational principles have inspired our thinking about the molecular role of the lipid bilayer in biological membranes. At the same time, NMR spectroscopy, and also spin-label electron paramagnetic resonance spectroscopy, has led our ideas about the dynamic features of the ordered membrane environment, as characterized by molecular order parameters. The representation of these features by MD calculations therefore extends our conceptual frame to wholescale membrane simulations.

To appreciate the power and potential problems of this latter approach, we should look back to the historical development as well as forward to future improvements (17). Early all-atom lipid force fields produced gel-like membranes above the chain-melting temperature, but this could be discovered only after sufficiently long simulations were possible (30). Up to that point, the area per lipid was severely underestimated in tension-free ensembles, and simulations were made at constant area instead of at constant pressure, thus limiting predictive ability and interpretative value in combination with diffraction techniques (31). Similarly, there have been continuous developments in nucleic-acid force fields, and good agreement (rmsd < 0.1 nm) with high-resolution DNA structure is obtained only with the most recent modifications (32). For folded proteins, different force fields reproduce similar structural ensembles (33–35), but further development was needed to treat intrinsically disordered proteins successfully (36).

It is clear that, although possibly subtle, adjustments in force fields are necessary to reproduce correct structural ensembles and conformer distributions for all biomolecular types. Modern experimental biophysics often relies on accurate and sufficiently long simulations to aid in the

interpretation of a variety of biophysical data, such as that from spin-label electron paramagnetic resonance (37–39), NMR (40–42), and Förster resonance energy transfer (43–45). It is therefore important to address the impact of force fields on the configurations of biomolecules, including lipid assemblies.

METHODS

Definition of dihedral angles and conformations

Fig. 1 *a* shows the notation used for the dihedral angles in *sn*-3 phosphatidylcholine, with explicit angles as listed in Table 1 (46). Dihedral angles are defined as in (47), which also is the current convention for protein structures (48). Fig. 1 *b* gives the classification of the staggered and eclipsed rotamers used for conformational description of lipids according to the range of dihedral angle (49). Equivalent conformational designations frequently used are as follows: *trans,* t (ap); *gauche,* g (sc); *skew,* s (ac); and *cis,* c (sp).

In the Pascher notation (2), the chain-backbone configuration is specified as θ_4/*leadingchain*/θ_2, where the leading chain is the one which proceeds directly into the bilayer from the attachment at the glycerol backbone.

MD simulations

We performed all-atom MD simulations of POPC bilayers using GROMACS v 5.1 (50–52) with the CHARMM36 (charmm36-jul2017.ff.tgz) (21) or BERGER (20) force field. The duration of the simulation trajectories used was 500 ns. The CHARMM bilayer contained 96 lipids. Trial simulations with 120 lipids did not result in any change in order parameters and dihedral distributions (data not shown). The Berger bilayer contained 120 lipids. The

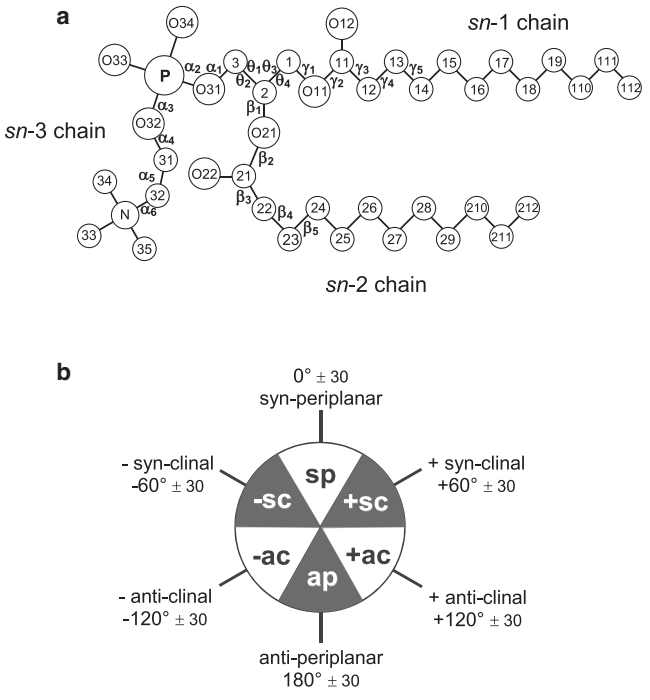

FIGURE 1 (*a*) Notation for dihedral angles in *sn*-3 diacyl phosphatidylcholine (46). (*b*) Designation of dihedral-angle ranges for staggered and eclipsed rotamers (49).

TABLE 1 Definition of Dihedral Angles

θ_1	O31−C3−C2−C1	β_1	C3−C2−O21−C21
θ_2	O31−C3−C2−O21	β_2	C2−O21−C21−C22
θ_3	C3−C2−C1−O11	β_3	O21−C21−C22−C23
θ_4	O21−C2−C1−O11	β_4	C21−C22−C23−C24
α_1	C2−C3−O31−P	γ_1	C2−C1−O11−C11
α_2	C3−O31−P−O32	γ_2	C1−O11−C11−C12
α_3	O31−P−O32−C31	γ_3	O11−C11−C12−C13
α_4	P−O32−C31−C32	γ_4	C11−C12−C13−C14
α_5	O32−C31−C32−N	–	–

Atom numbering is taken from Fig. 1.

water models used were the CHARMM version of TIP3P (53) and SPC (54), for CHARMM and Berger force fields, respectively. The LINCS algorithm (55) was used to constrain all bonds in the Berger simulations, and bonds containing hydrogen in the CHARMM simulations. The leapfrog integrator was used with a time step of 2 fs.

For the Berger force field, simulations were carried out with standard parameters as described in (56). A neighbor list with a 1.0 nm cutoff was used for nonbonded interactions and was updated every 10 steps. van der Waals interactions were truncated with a cutoff of 1.0 nm. The particle mesh Ewald method with a 0.12-nm Fourier spacing and 1.0-nm short-range cutoff was used for electrostatic interactions (57,58). Temperature and semiisotropic pressure coupling was performed using the Berendsen thermostat and barostat (59). Trajectories were sampled every 10 ps.

For CHARMM simulations, particle mesh Ewald had a short-range cutoff of 1.2 nm, and van der Waals interactions were switched off over the range from 1.0 to 1.2 nm. The Nose-Hoover thermostat was used (60). Parrinello-Rahman (61) pressure coupling was used for production runs after equilibrating the systems with Berendsen pressure coupling.

Order parameters

The ^{2}H-quadrupole splitting of the perpendicular peaks in a Pake doublet is as follows:

$$\Delta\nu_Q = \frac{3}{4}\left(\frac{e^2qQ}{h}\right)S_{\mathrm{CD}}, \qquad (1)$$

where $e^2qQ/h = 163$ kHz for an aliphatic C−D bond (62) and S_{CD} is the order parameter of the C−D bond referred to the membrane normal. Because rotation is rapid about the N−C bond of choline methyls, their C−D or (C−H) order parameter is $S_{\mathrm{CD_3}} = -(1/3)S_{\mathrm{NC}}$ where S_{NC} is the order parameter of the three equivalent N−C33, N−C34, and N−C35 bonds. The effective quadrupole coupling for rapidly rotating CD_3 methyls is $\frac{1}{3}e^2qQ/h = 46$ kHz (62); both this and the CD_2 value are from the crystalline lamellar phase (L_c) of a phospholipid with perdeuterated chains (10).

The order parameter S_{CN} of the C32−N bond measured by ^{14}N-NMR is related directly to the choline methyl CD_3 order parameter (63):

$$S_{\mathrm{CN}} = \frac{S_{\mathrm{NC}}}{\frac{1}{2}(3\cos^2\theta_{\mathrm{CNC}} - 1)} = \frac{-3S_{\mathrm{CD_3}}}{\frac{1}{2}(3\cos^2\theta_{\mathrm{CNC}} - 1)}, \qquad (2)$$

where $\theta_{\mathrm{CNC}} = 111.3^{\circ}$ (4,64) is the mean C32-N-C33, -C34, and -C35 choline bond angle. Using the value of $S_{\mathrm{CD_3}}$ for dipalmitoyl phosphatidylcholine (PC) at 317 K from Ref. (63) with the corresponding value of S_{CN} from ^{14}N-NMR (65), we deduce a ^{14}N-quadrupole coupling of $e^2qQ/h = 119$ kHz from Eqs. 1 and 2.

The ^{31}P chemical shift anisotropy (csa) with axial averaging is (66):

$$\Delta\sigma_{csa} = (\sigma_{11} - \sigma_{22})S_{11} + (\sigma_{33} - \sigma_{22})S_{33}, \quad (3)$$

where $(\sigma_{11} - \sigma_{22}) = -62$ ppm and $(\sigma_{33} - \sigma_{22}) = 134$ ppm for hydrated dimyristoyl PC at 248 K (67); S_{11} and S_{33} are the order parameters of the csa-principal axes, which lie close to the O31−O32 and O33−O34 vectors, respectively, of the phosphate diester. An approximate model relates the chemical shift anisotropy to the value $\Delta\sigma_R$ obtained simply by uniaxial rotation about the principal molecular axis (68):

$$\Delta\sigma_{csa} = \Delta\sigma_R S_{PO_4}, \quad (4)$$

where S_{PO_4} is the order parameter of this principal axis relative to the membrane normal. A reasonable estimate for rotational averaging is $\Delta\sigma_R = -74$ ppm, which we get by using the value of $\Delta\sigma_{csa}$ from the gel phase (62, and see also 69). Typical errors in $\Delta\sigma_{csa}$ are ± 1 ppm or better (70).

Motionally averaged ^{1}H-^{13}C dipolar couplings are determined by

$$\langle b_{CH}\rangle = -\left(\frac{\mu_o}{4\pi}\right)\frac{\hbar\gamma_C\gamma_H}{r_{CH}^3}S_{CH}, \quad (5)$$

where the rigid-limit dipolar coupling is $(\mu_o/4\pi)(\hbar\gamma_C\gamma_H/r_{CH}^3) = 20.2$ kHz (71) and S_{CH} is the order parameter of the C−H bond. Typical errors in recoupled dipolar frequencies are ± 0.4 kHz (71) or larger (72), whereas those from direct measurement of ^{31}P-csa or quadrupole splittings are typically $\pm(0.1-0.2)$ kHz, including those for ^{14}N (65,70).

RESULTS

Headgroup conformation

Fig. 2 shows the distributions of dihedral angles in the polar headgroups for the Berger et al. (*dotted line*) and CHARMM36 (*solid line*) force fields. Results for α_5 are similar to those reported previously by Botan et al. (29). There are clear differences between simulation results from the two force fields, particularly as regards the α_1 and α_4 dihedrals. Significantly, the distributions for both are identical for the Berger force field, whereas they differ considerably from one another for the CHARMM36 force field. On the other hand, the distributions of α_2 and α_3 dihedrals are more similar both to each other and between the two force fields. Differences within the α_1/α_4 and α_2/α_3 pairs must reflect differences in nonbonded interactions beyond those between immediate pendant groups.

Table 2 lists the distribution of headgroup dihedrals binned into $\pm 30°$ ranges about the staggered and eclipsed positions for sp^3-bonds, as in Fig. 1 *b*. These are compared with distributions found from crystal structures available for glycerophospholipids, namely phosphatidylcholine, phosphatidylethanolamine, mono- and dimethylphosphatidylethanolamine, phosphatidic acid, and phosphatidylglycerol.

We see that the headgroup conformation for the Berger force field is predominantly α_1 = ap, $\alpha_2 = \pm$sc, $\alpha_3 = \pm$sc, α_4 = ap, and $\alpha_5 = \mp$ sc but with a comparable contribution from ap. This is close to that found in bilayer crystals, except for the ap component of α_5, which occurs in crystals only for phosphatidylglycerol. Berger et al. retain the original GROMOS force field for the headgroup bonded interactions, and use OPLS for nonbonded Lennard-Jones interactions. In earlier simulations of fluid dipalmitoyl PC bilayers using the GROMOS force field, but with reduced atomic charges, Egberts et al. (19) also find choline headgroup rotamers similar to those in lipid crystals. For CHARMM36, the headgroup conformation is less like that of phosphatidylcholine bilayer crystals, predominantly α_1 = ap and −ac, $\alpha_2 = \pm$sc, $\alpha_3 = \pm$sc, $\alpha_4 = \pm$sc, and $\alpha_5 = \pm$sc. These conformational deviations exhibited by the MD simulations may diminish the internal electrostatic attraction that directs the positively charged nitrogen to the phosphate oxygens in the crystal structures. Also, we must remember that the phosphocholine headgroup occupies a larger cross-sectional area than the crystalline chains. This is accommodated by tilting the chains in the crystal, as in phosphatidylcholine gel phases. Note that a correlated $\alpha_2/\alpha_3 = \pm$sc/$\pm$sc conformation is expected on energetic grounds for a phosphate diester (73). As seen

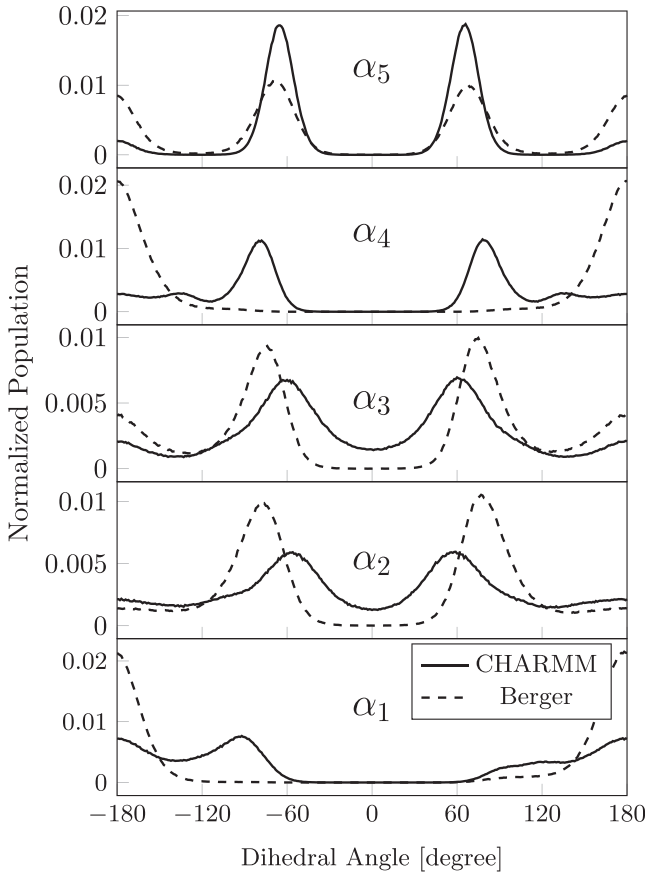

FIGURE 2 Distribution of dihedral angles in the polar headgroup of POPC. From bottom to top: α_1 about the C3−O31 bond, α_2 about the O31−P bond, α_3 about the P−O32 bond, α_4 about the O32−C31 bond, and α_5 about the C31−C32 bond. CHARMM force field (*solid line*) and that of Berger et al. (*dotted line*).

TABLE 2 Conformation of Polar Headgroup in MD Simulations of POPC

Dihedral		ap	sc	−sc	ac	−ac	sp
α_1	Berger	0.865	0.010	0.001	0.103	0.041	0
	CHARMM	0.359	0.028	0.130	0.190	0.294	0
	crystal	0.79	0	0	0.10	0.10	0
α_2	Berger	0.079	0.307	0.300	0.159	0.151	0.002
	CHARMM	0.120	0.274	0.270	0.110	0.118	0.107
	crystal	0	0.60	0.40	0	0	0
α_3	Berger	0.188	0.285	0.272	0.132	0.122	0.001
	CHARMM	0.099	0.303	0.302	0.093	0.091	0.112
	crystal	0	0.64	0.36	0	0	0
α_4	Berger	0.833	0.003	0.004	0.078	0.082	0
	CHARMM	0.152	0.252	0.257	0.172	0.166	0.000
	crystal	0.21	0	0	0.57	0.21	0
α_5	Berger	0.286	0.306	0.330	0.036	0.037	0.003
	CHARMM	0.062	0.461	0.462	0.007	0.006	0.001
	crystal	0.14	0.50	0.29	0	0.07	0

Top row for each dihedral angle α is with force field of Berger et al. (20), middle row is with CHARMM C36 force field (21), and bottom row is the average population in crystal structures of glycerophospholipids (4).

in Fig. 2 and Table 2, the relative populations of α_2 and α_3 are consistent with this pairing, for both force fields. Raman spectroscopy shows that torsion angle α_5 is predominantly $\mp$sc in hydrated phosphatidylcholine bilayers (74), as predicted with both force fields.

Correlations between adjacent dihedral angles α_i/α_{i+1} in the headgroup are shown by the doublet distributions that are given in Fig. 3. In the second column, we see very clearly that $\alpha_2/\alpha_3 = \pm$sc/$\pm$sc as expected, for both force fields. For the CHARMM36 force field, we get the correlated sequence $\alpha_2/\alpha_3/\alpha_4/\alpha_5 = \pm$sc/$\pm$sc/$\pm$sc/$\pm$sc, without sign reversal for α_5. For the force field of Berger et al., the correlated sequence is predominantly $\alpha_2/\alpha_3/\alpha_4/\alpha_5 = \pm$sc/$\pm$sc/ap/$\mp$sc, with sign reversal for α_5, where we use the doublet distribution α_3/α_5 (data not shown) to bridge the ap conformation of α_4.

Glycerol backbone

The θ_4 dihedral angle, about the glycerol C1−C2 bond, specifies the relative orientation of the *sn*-1 and *sn*-2 chains. Correspondingly, the θ_2-dihedral, about C2−C3, defines the orientation of the headgroup relative to the *sn*-2 chain. The θ_3/θ_1 combination of complementary dihedral angles specifies the glycerol configuration. For tetrahedral bond angles, the complementary dihedral angles of *sn*-3 glycerol are related by $\theta_1 = \theta_2 - 120^o$ and $\theta_3 = \theta_4 + 120^o$.

Fig. 4 compares distributions of the θ_2 and θ_4 dihedrals (*solid lines*) with their complements $\theta_1 + 120^o$ and $\theta_3 - 120^o$ (*dotted lines*). Results for θ_3 are similar to those reported previously by Botan et al. (29). Displacements of the solid and dotted lines by $\approx \pm 8°$, respectively, with the Berger force field indicate departures from strictly tetrahedral geometry, or an insufficient constraint on the improper dihedrals that maintain the enantiomeric configuration of the backbone. For the CHARMM force field, however, the complementary pairs of dihedrals coincide as expected. The major peaks in population differ considerably between the two force fields. For the Berger force field they occur close to $\theta_2 = 180^o$ (*trans*, ap), $\theta_2 = 60^o$ (*gauche*$^+$, sc), and to $\theta_4 = \pm 60^o$ (*gauche*$^\pm$, $\pm$sc), but with significant deviations (∼5–10°) from the canonical staggered positions for sp^3-bond dihedrals of glycerol. In addition, the θ_4-distribution has a further peak at 158°. On the other hand, the CHARMM force field produces two major peaks in population at θ_2 and $\theta_4 = \pm 60^o$, with only a minor contribution in the *trans* region.

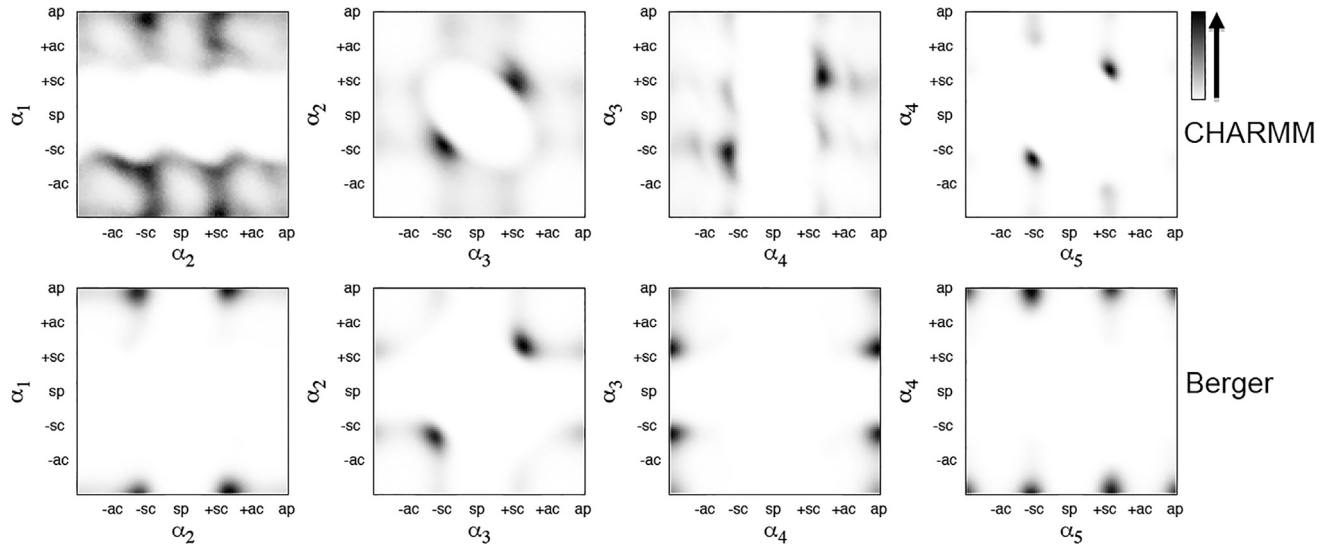

FIGURE 3 Doublet distributions for pairs of adjacent headgroup dihedrals α_i/α_{i+1}, from simulations with the CHARMM force field (*upper row*) and that of Berger et al. (*lower row*).

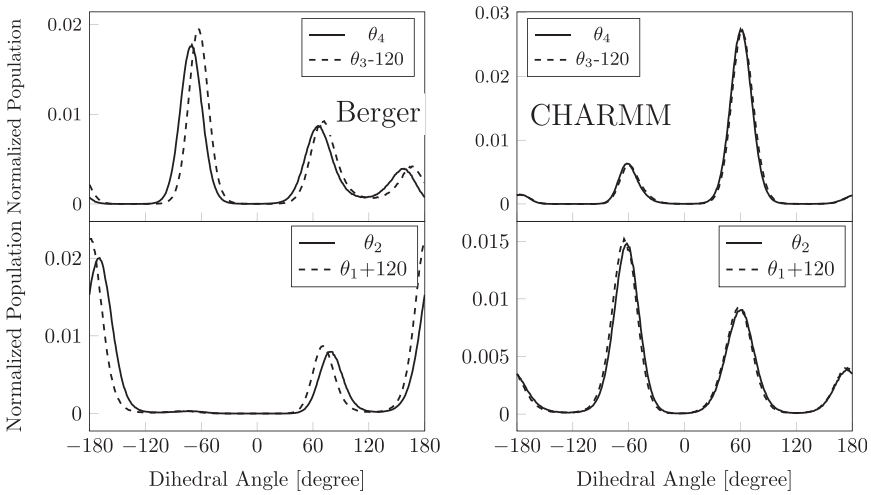

FIGURE 4 Distribution of dihedral angles in the glycerol backbone of POPC. Top: the C2−C3 bond θ_2 (*solid line*) and θ_1+120° (*dotted line*). Bottom: the C1−C2 bond θ_4 (*solid line*) and θ_3−120° (*dotted line*). CHARMM force field (*right*) and that of Berger et al. (*left*).

Table 3 lists the distribution of backbone dihedrals grouped in ±30° ranges about the staggered and eclipsed positions for C−C bonds (see Fig. 1 *b*). Again, comparison is made with distributions from the available range of crystal structures (4). The θ_4-dihedral is 50% −sc, 29% sc, and 9% ap (12% eclipsed) for the Berger force field, and 16% −sc, 78% sc, and 4% ap (2% eclipsed) for CHARMM36. Only backbones with θ_4 = +sc or −sc allow parallel chain stacking characteristic of a membrane bilayer arrangement. The θ_2-dihedral is 66% ap, 19% sc, and 1% −sc (14% eclipsed) for the Berger force field, and 14% ap, 32% sc, and 48% −sc (6% eclipsed) for CHARMM36. Backbones with ±sc conformations for θ_4 and θ_2 are favored by the "*gauche* effect" found in polyoxyethylene (75). However, combinations of θ_4/θ_2 dihedral angles −sc/sc, and sc/−sc with *sn*-2 as the leading chain, are excluded because each would rotate the headgroup back into the bilayer, and the former also exhibits a sterically forbidden $\theta_3/\theta_1 = g^+g^-$ glycerol configuration (2). For a similar reason, the θ_4/θ_2 = ap/ap configuration (with $\theta_3/\theta_1 = g^-g^+$) is also strongly disfavored on intramolecular grounds. The values in Table 3 allow the favorable combinations θ_4/θ_2 = −sc/ap, sc/sc, and sc/ap with diminishing frequency for the Berger force field, and predominantly sc/−sc and sc/sc for CHARMM36. Of these, the sc/−sc and sc/sc combinations are strongly represented in the available crystal structures, and those involving ap conformers considerably less so. Correspondingly, the potential energy wells in CHARMM36 are deepest for θ_4/θ_2 = sc/−sc and sc/sc, and are less deep for sc/ap, ap/−sc, −sc/−sc, and −sc/ap (21).

Fig. 5 shows the doublet distribution θ_2/θ_4 that confirms the above correlations, which were based on relative populations. For CHARMM36, we get θ_4/θ_2 = +sc/±sc with small contributions from sc/ap and −sc/−sc. For the Berger force field, we find predominantly θ_4/θ_2 = −sc/ap, with smaller contributions from sc/sc, sc/ap, and ap/sc.

Chain attachment

Fig. 6 shows the distributions of dihedral angles about the first four bonds in the attachment of the *sn*-1 and *sn*-2 acyl chains. For β_1, γ_1 and β_3, γ_3, there are considerable differences between the dihedral distributions produced by the two force fields. Steric interactions arising from torsion about the C−O bond restricts β_1 and γ_1 less than for C−C bonds (76). This makes differences between the two force fields difficult to interpret unambiguously for the first dihedral. The unique ap conformation for β_2 and γ_2 that is found with both force fields reflects the planar nature of the carboxyl ester, and is a feature common to all known bilayer phospholipid crystal structures (see Table 3). The subsequent β_3 and γ_3 C−C dihedrals specify which of the acyl chains, if any, is the leading chain. For γ_3 = ap, *sn*-1 is the leading chain, and correspondingly for β_3 = ap, *sn*-2 is the leading chain. Although either γ_3 or β_3 is in the ap conformation in phospholipid crystals, this is certainly not the case for simulations with the Berger force field (see Fig. 6; Table 3). Compared with bilayer crystal structures, the wide dihedral distribution for γ_3 and β_3 with maxima at approximately ±90° for the Berger force field is highly unusual. Moreover, the reflection symmetry of the two distributions indicates equivalence of the two chains. For the CHARMM36 force field, on the other hand, γ_3 is mostly ap, which indicates that *sn*-1 is the leading chain, and β_3 has a considerable –sc population, which favors a bent *sn*-2 chain.

The ap (*trans*) and mostly less populated ±sc (*gauche*) conformations for β_4 and γ_4 are characteristic of fluid lipid hydrocarbon chains, and persist throughout the remainder of the two chains except in the region of the 9,10-*cis* double bond of the *sn*-2 chain. This applies for both force fields.

Acyl chains

Fig. 7 shows the profile of rotamer populations in the *sn*-1 and *sn*-2 acyl chains. After the bonds that characterize the

TABLE 3 Conformations of Glycerol Backbone and Chain Carboxyl Links in MD Simulations of POPC

Dihedral		ap	sc	−sc	ac	−ac	sp
Backbone							
θ_1	Berger	0.009	0.695	0.233	0.025	0.000	0.037
	CHARMM	0.484	0.133	0.319	0.025	0.019	0.018
	crystal	0.45	0.14	0.36	0	0	0.05
θ_2	Berger	0.657	0.194	0.010	0.068	0.071	0
	CHARMM	0.138	0.323	0.476	0.020	0.023	0.019
	crystal	0.15	0.45	0.40	0	0	0
θ_3	Berger	0.285	0.514	0.116	0.003	0.078	0.004
	CHARMM	0.783	0.158	0.038	0.008	0.013	0.000
	crystal	0.76	0.24	0	0	0	0
θ_4	Berger	0.091	0.293	0.498	0.089	0.025	0.004
	CHARMM	0.040	0.778	0.163	0.009	0.000	0.008
	crystal	0	0.74	0.26	0	0	0
Chains							
β_1	Berger	0.192	0.472	0.022	0.312	0.001	0.000
	CHARMM	0.271	0.362	0.005	0.362	0	0.000
	crystal	0.33	0.25	0	0.42	0	0
β_2	Berger	0.970	0	0	0.022	0.003	0.004
	CHARMM	0.992	0	0	0.005	0.003	0
	crystal	1.0	0	0	0	0	0
β_3	Berger	0.100	0.105	0.308	0.110	0.303	0.077
	CHARMM	0.374	0.015	0.214	0.037	0.334	0.024
	crystal	0.46	0	0.36	0	0.18	0
β_4	Berger	0.760	0.089	0.083	0.034	0.032	0.000
	CHARMM	0.422	0.314	0.173	0.059	0.031	0.000
	crystal	0.73	0.27	0	0	0	0
γ_1	Berger	0.749	0.046	0.014	0.091	0.099	0.000
	CHARMM	0.171	0.313	0.065	0.219	0.232	0
	crystal	0.54	0.05	0	0.32	0.09	0
γ_2	Berger	0.979	0	0	0.006	0.014	0
	CHARMM	0.995	0	0	0.002	0.003	0
	crystal	1.0	0	0	0	0	0
γ_3	Berger	0.119	0.209	0.167	0.260	0.184	0.061
	CHARMM	0.417	0.103	0.113	0.153	0.166	0.048
	crystal	0.73	0.09	0.04	0.09	0.04	0
γ_4	Berger	0.755	0.087	0.091	0.032	0.034	0.000
	CHARMM	0.646	0.141	0.133	0.041	0.038	0
	crystal	0.86	0.09	0.04	0	0	0

Top row for each dihedral angle θ, β, γ is with force field of Berger et al. (20), middle row is with CHARMM C36 force field (21), and bottom row is population in crystal structures of glycerophospholipids (4).

chain attachment, the populations of *trans* and *gauche* rotamers remain approximately constant throughout the length of the *sn*-1 chain. We see a similar pattern in the *sn*-2 chain except for bonds that immediately surround the 9,10-*cis* double bond, which are in *skew* (s) conformations. Quasi straight-chain packing about the double bond (Δ) arises with rotamer sequences such as $g^+s^+\Delta s^+$ (77). Beyond the fourth bond, the chain profiles are similar for both force fields, with only slight quantitative differences in conformational populations. The dips in population profiles where *gauche* or *trans* conformations are replaced by *skew* conformations are directly reflected in the order profiles for the *sn*-2 chain that are presented in Fig. S1.

DISCUSSION

The conformational populations given here represent the combined effects of both nonbonded interactions and torsional potentials in the corresponding force field. In addition, harmonic constraints maintain the *cis* configuration of the oleoyl chain and planarity of the carboxyl groups. The glycerol backbone is similarly restrained in the Berger force field to give the correct enantiomer. Correct stereochemistry is thereby achieved with both force fields, but considerable differences are found in the conformational distributions. The results raise two important general issues. Can the two force fields describe the universal *sn*-1/*sn*-2 chain inequivalence that characterizes molecular packing in tension-free fluid bilayers of *sn*-3 glycerophospholipids? Furthermore, to what extent do the MD conformations agree with the combined data from crystal structures of glycerophospholipids and spectroscopic (NMR and infrared) studies of their fluid-bilayer phases?

Headgroup conformation

Comparison of the headgroup conformation from MD simulations with those found in bilayer crystals is significant. This is because deuterium and phosphorus NMR anisotropies (or order parameters) can be explained by rapid interconversion between two mirror-image configurations that are related to those observed in glycerophosphocholine crystals (11,12,78). The two-enantiomer interpretation has been questioned as being oversimplified (79), but until now this has not been tested. Therefore, a detailed examination of headgroup configurations is warranted here. The polar-group structure produced by simulations with the Berger force field is that of the crystal conformation DMPC B (dimyristoyl phosphatidylcholine B) of the complete phosphatidylcholine molecule, whereas that from the CHARMM36 force field is closer to glycerophosphocholine alone.

A direct experimental check on whether conformations predicted by simulation are appropriate to fluid hydrated bilayers comes from calculating explicitly the order parameters that we measure from NMR. The right panel of Fig. 8 gives the C−H (or C−D) order parameters for the C31 and C32 atoms, and the three equivalent C33−C35 methyl atoms. Experimental data for POPC are given by open symbols, with that from egg PC by the right-pointing triangle. The diastereotopic H-atoms of prochiral C31 and C32 methylenes (47) are dynamically near equivalent. Acceptable dynamic structures should therefore predict these experimentally observed equivalences. The order parameters predicted by CHARMM36 simulations (*solid lines*) describe the experimental measurements quite well. In contrast to the Berger force field (*dashed lines*), they predict the correct sign for the C32−H order parameter and for that of C33−H to C35−H. Otherwise, the Berger force field reproduces the measured C31−H order parameter reasonably

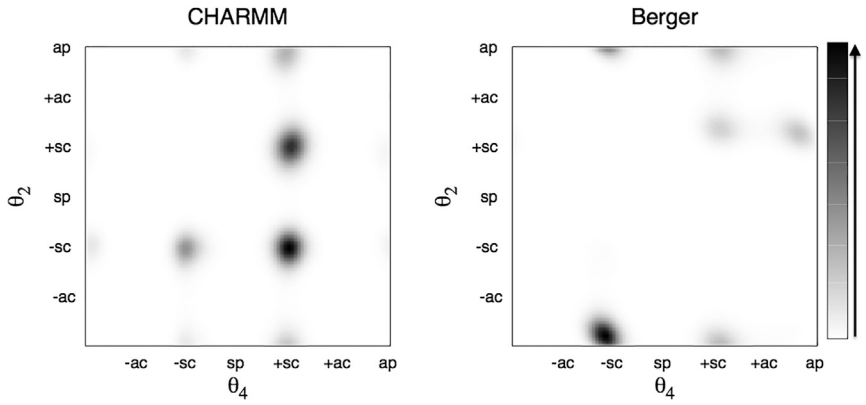

FIGURE 5 Doublet distributions for the pair of backbone dihedrals θ_2/θ_4 from simulations with the CHARMM force field (*left*) and that of Berger et al. (*right*).

well. Because the Berger force field uses united atoms, we introduced C−H vectors for these calculations at the tetrahedral angles specified by the positions of the united (i.e., heavy) atoms.

The order parameter S_{CN} of the C32−N bond that is measured by ^{14}N-NMR is related directly to the choline methyl CD_3 order parameter (as explained in Methods) but is much larger in size. The right panel of Fig. 8 compares MD predictions with the experimental values for POPC. CHARMM36 produces much better agreement than does the Berger force field, as in the case of the C32−H and CD_3 order parameters. Uncertainties in order parameters from these measurements are no larger than the open symbols. The prediction from CHARMM36 is close to the experimental values, but still lies outside the estimated error range.

The order parameters for the principal axes of the ^{31}P-phosphate diester chemical shift anisotropy are $S_{11} = 0.165$, 0.058 (O31−O32) and $S_{33} = -0.227$, -0.105 (O33−O34) from CHARMM36 and the Berger force field, respectively. From Eq. 3 we then predict measured chemical shift anisotropies: $\Delta\sigma_{csa} = -41$ ppm, and -18 ppm for CHARMM36 and Berger, respectively. These are smaller (in absolute terms) than the experimental values for POPC of -47 ± 0.5 ppm at 298 and 303 K (80,81) and -49.4 ppm at 288 K (82). However, the prediction from CHARMM36 is much closer than that from the force field of Berger et al. These calculations depend somewhat on the principal values chosen for the csa tensor. Values of the S_{PO_4} order parameter derived from Eq. 4 are included in the comparison of simulation with experiment that we show in Fig. 8; the uncertainty is less than the size of the symbols, and the CHARMM prediction lies well outside this.

An extensive survey of different force fields shows that CHARMM36 is best at predicting C31−H and C32−H order parameters of the choline headgroup and the only one to give the correct sign for C32−H (29). In this work and a later review (83), it was concluded that one must improve existing force fields for the choline headgroup and also the glycerol backbone. However, the two choline S_{CH} order parameters considered by no means sample all dihedral angles of the phosphocholine headgroup, e.g., the relative sign of α_5. Comparison with the phosphatidylcholine crystal conformation (see above) shows that CHARMM36 predictions for fluid membranes differ in the α_4 dihedral and in the sense of α_5. Interpretation of C−D order parameters from fluid-phase dipalmitoyl PC bilayers suggests that α_4 is in a $\pm$ ac conformation and that α_5 might assume either relative sign (78). On the other hand, C−D order parameters from POPC bicelles at 35°C are well fitted by a single $\alpha_3/\alpha_4/\alpha_5 = -$sc/ap/+sc conformation, coupled to rapid axial rotation (84). Further force field development clearly should include the entire phosphocholine headgroup, making use of ^{31}P-csa and quadrupole splittings of ^{14}N and choline CD_3 groups, as is done here.

Glycerol backbone and chain attachment

The conformations of the glycerol backbone produced by the CHARMM36 force field are closer to those of the majority species in crystal structures than are those produced by the force field of Berger et al. This consensus configuration also corresponds to one of the conformers sc/*sn*-1/−sc found in bilayer crystals of dimyristoyl *sn*-3 phosphatidylcholine (viz., DMPC B) (64). The other is sc/*sn*-1/ap (viz., DMPC A), which appears weakly with the Berger force field.

The *sn*-1 and *sn*-2 chains are equivalent with the Berger force field, which therefore produces no leading chain. In contrast, CHARMM36 simulations produce chain inequivalence with *sn*-1 as the leading chain, as established experimentally from measurement of deuterium-NMR order parameters S_{CD} (8,9). This is not entirely surprising, because the β_1, θ_4, and θ_2 potential surfaces in CHARMM36 are optimized empirically to fit the anomalous S_{CD} for C-2 of the *sn*-2 chain (i.e., C22), which is the hallmark of fluid-phase chain inequivalence (21). Indeed, CHARMM36 is the only force field so far to produce inequivalent order parameters for the two C-2 deuterons. Chain order-parameter profiles from both force fields are shown in Fig. S1. These confirm the above remarks. In particular, *sn*-1 is the leading chain

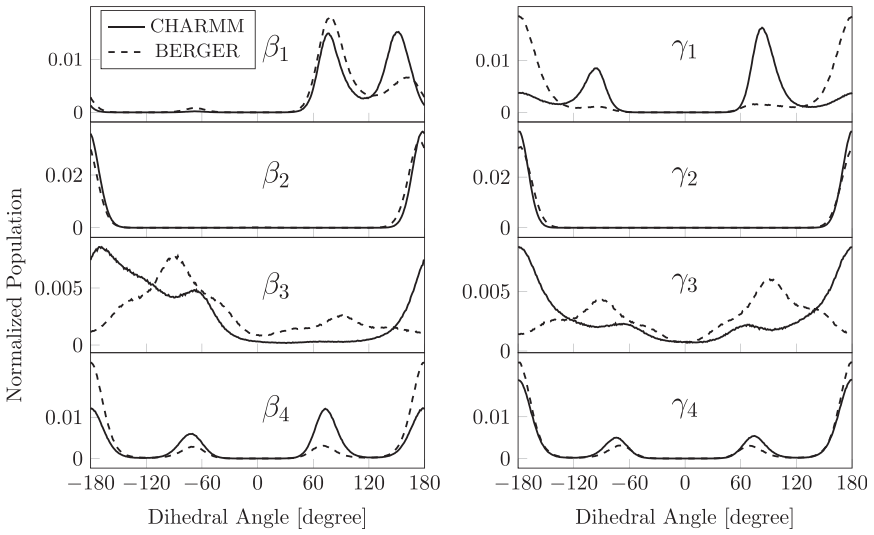

FIGURE 6 Distribution of dihedral angles at the carboxyl end of the POPC chains. Left *sn*-2 chain: β_1 about the C2−O21 bond, β_2 about the O21−C21 bond, β_3 about the C21−C22 bond, and β_4 about the C22−C23 bond. Right *sn*-1 chain: γ_1 about the C1−O11 bond, γ_2 about the O11−C11 bond, γ_3 about the C11−C12 bond, and γ_4 about the C12−C13 bond. CHARMM force field (*solid line*) and that of Berger et al. (*dotted line*).

in the CHARMM36 simulation, and $-S_{CD}$ for the C-2 methylene of the *sn*-2 chain is much smaller than for *sn*-1, although the inequivalence between the two C−D bonds is less than that found experimentally. It is no larger than predicted by CHARMM36 for C-2 at *sn*-1; after adding H-atoms, the Berger et al. force field predicts negligible inequivalence. Also, order profiles down the chain differ in detail between the CHARMM36 and Berger force fields. Comparison of MD-simulated profiles with experimental chain order parameters of POPC are shown already in (21,85).

The unusual symmetrical chain packing configuration of the Berger lipids may be responsible for overbinding of Na^+ ions. Fluid-bilayer simulations with the Berger et al. force field predict Na^+ binding to the carboxyl ester groups of phosphatidylcholine (see 25,27,86; and references therein). Experimental studies, however, exclude the possibility that Na^+ binds significantly to phosphatidylcholine bilayers (4). The electrophoretic mobility of pure phosphatidylcholine vesicles is very low, independent of NaCl concentration (87,88). Experimental estimates for the Na^+ association constant are 0.15 M^{-1} (89,90), which puts the dissociation constant at a concentration above the maximal solubility of NaCl in water. Comparing the partial atomic charges of the Berger et al. force field with those of CHARMM36 (see Table S1) reveals a considerably higher negative charge on the ester oxygens for the Berger force field, in addition to the difference in chain accessibility. Note, however, that a small increase in radius for the Lennard-Jones O−Na^+ interaction in CHARMM36 is still needed to reduce residual binding to POPC (26; see also Ref. 27 in the Supporting Material).

The left panel of Fig. 8 gives the C−H order parameters for the C1−C3 atoms of the glycerol backbone. Experimental values are shown as open symbols. The *pro-R* and *pro-S* H-atoms attached at C1, and to a lesser extent those at C3, are inequivalent (47). Predictions from CHARMM36 simulations (*solid line*) agree rather well with the experimental order parameters, particularly the difference between the diastereomers for C1−H. We expect this from the good agreement with the backbone conformation in bilayer crystals and the fact that CHARMM36 is specifically tailored to reproduce the *sn*-1/*sn*-2 chain inequivalence (see above). There is little agreement between experiment and predictions for the glycerol backbone from the Berger force field (*dashed line*), as we anticipate from the very different conformation produced by using this approach (see above). These differences between predictions for the glycerol-backbone order parameters are indeed found for a much wider range of lipid force fields (29,83). As already mentioned, the latter authors conclude that further improvements in force fields could help to match the backbone order parameters better.

Chain conformation

Both force fields agree in predicting a relatively constant rotamer population throughout the length of the hydrocarbon chain, except close to the *cis* double bond of the *sn*-2 oleoyl chain. The well-known chain-order-parameter profile (see Fig. S1) is the cumulative effect of these *gauche* rotamers down the chain. In total, the *sn*-1 chain (γ_4−γ_{15}) contains approximately 3.1 *gauche* rotamers using CHARMM36 (2.6 from Berger), with a roughly equal distribution between g^+ and g^-: $p_{g^\pm} \approx 0.13 \pm 0.004$ (0.11 for Berger). Outside the region of the double bond, the *gauche* probability in the *sn*-2 chain (β_4−β_8, β_{14}−β_{17}) is similar to that in the *sn*-1 chain: $p_{g^\pm} \approx 0.13 - 0.15 \pm 0.02$ (0.11 for Berger). These values are in the region of earlier statistical mechanical estimates using the isomeric state model (91,92) and more recent spectroscopic measurements (reviewed in 93; see also 94–96). The differences in *gauche* probability between CHARMM36 and Berger are reflected in the different chain-order profiles for these two force fields that are shown

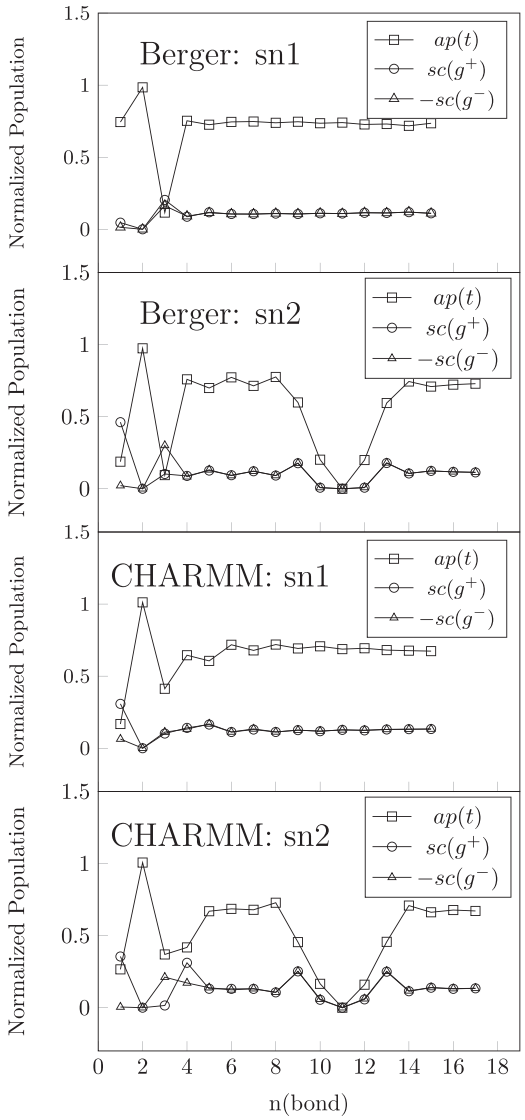

FIGURE 7 Chain profiles of *trans* (ap, *squares*) and *gauche*$^{\pm}$ (+sc, *circles*; −sc, *triangles*) conformational populations of POPC. CHARMM force field (*right*) and that of Berger et al. (*left*). Top: *sn*-1 chain (γ_n-dihedrals); bottom: *sn*-2 chain (β_n-dihedrals).

in Fig. S1. Although the probability of an individual *gauche* conformation does not vary greatly along the chain, the cumulative effect at a given chain segment depends on the absolute value of p_g. Also, the probability of higher-order combinations of neighboring *gauche* conformations increases on proceeding down the chain.

Unlike the lipid structures in the PDB to which we referred in the Introduction, none of the chains from MD simulations are in high-energy eclipsed conformations, even for the united-atom force field.

CONCLUSION

The ultimate aim of atomistic MD is to describe the properties of membranes by the behavior of real lipid molecules. Only then can we access all properties down to the shortest scales. To do this, the constituent lipids must have realistic molecular structures that conform to the configurational and packing principles established in lipid crystals. This a fundamental question of wide and general interest that lies at the heart of molecular approaches to biophysics.

The dynamic lipid structures produced by MD simulations display none of the conformational irregularities that are a frequent feature of lipid structures deposited in the PDB (5–7). Nevertheless, the two popular force fields used here differ in the structures predicted, particularly for the phosphatidylcholine polar headgroup and the glycerol backbone. Not surprisingly, CHARMM36 performs extremely well for the backbone, for which it specifically is optimized. The situation for the polar group is more interesting. The S_{CH} order parameters and the S_{CN} order parameter, and the ^{31}P-csa, are all reproduced quite well by CHARMM36; most importantly, this includes the signs (see Fig. 8). The predicted α_4 dihedral is not that found in the favored phosphatidylcholine crystal structure (DMPC B), nor that used in one case to describe order parameters of the POPC headgroup (84). However, $\alpha_4 = \pm$ac is the dihedral used originally for interpreting the order parameters, which were based on the crystal structure of glycerophosphocholine, not that of phosphatidylcholine (11,78). Note that the set of α-dihedral values used originally (11) predicted the negative sign of S_{CH} for C32 correctly, before this was established experimentally. The relative sign predicted for α_5 by CHARMM36 is that found in the phosphatidylethanolamine headgroup, not that in the crystal structure of phosphatidylcholine (see, e.g., 4,6), nor that used originally for the phosphatidylcholine order parameters (11). This is probably related to difficulties in packing choline headgroups in bilayer crystals, which are alleviated in fluid bilayers.

The success of CHARMM36 in accounting for the whole range of experimentally available headgroup order parameters in Fig. 8 suggests that the original interpretation of the ^{2}H-NMR results in terms of exchange between two mirror-image headgroup conformations could be substantially correct. This is because the dihedral distributions in Figs. 2 and 3 are predominantly symmetrical, and hence approximately consistent with interconverting enantiomers. The detailed conformational populations differ, and more work would be useful to test the predictions of headgroup conformation from MD simulations with different force fields. It would help to concentrate further on the extended range of headgroup order parameters, i.e., including ^{31}P-csa and S_{CN} (or S_{CD_3}) as experimental targets for validation in force field development. The phosphate group, in particular, is central to the dynamic behavior of the entire lipid molecule because it is located directly at the interface between polar and hydrophobic regions, and reflects the angular fluctuations of the whole molecule (68). Because of the close link between molecular conformation and bilayer dimensions,

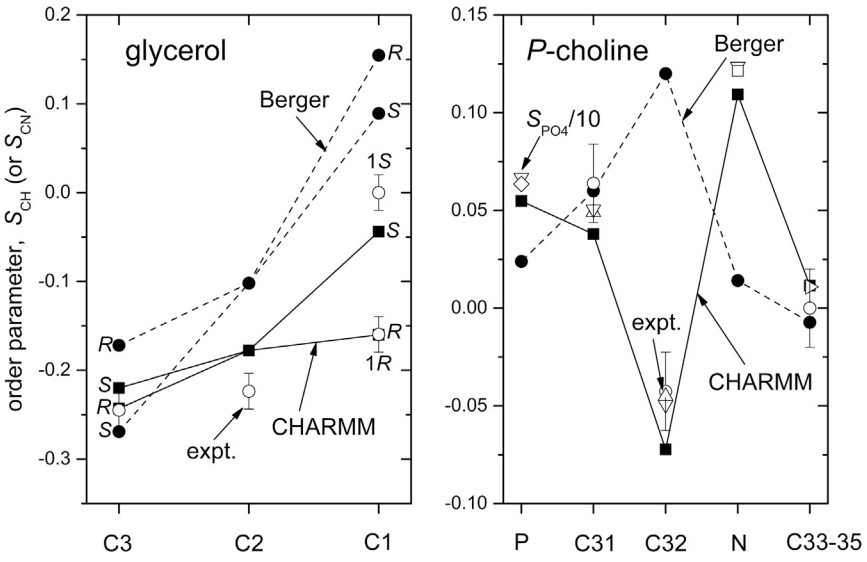

FIGURE 8 Order parameter of the C−H (or C−D) bond in the headgroup (*right panel*) and glycerol backbone (*left panel*). Values for the C32−N bond and the phosphate group (×0.1) are also included. The C3 and C1 methylenes are prochiral with dynamically distinguishable *pro-R* and *pro-S* H-atoms (47); experimental assignments (1*R*, 1*S*) are from Ref. (97). The two H-atoms on C31 and C32 are dynamically equivalent. Open symbols are experimental values for POPC (*circles*: Ref. (85), at 300 K; *triangles*: Ref. (98), at 296 K; *inverted triangles*: Ref. (82), at 288 K; *square*: Ref. (70) at 308 K; *diamond*: Refs. (80,81), at 299, 303 K), except the right triangle is for egg PC (Ref. (99), at 303 K). Signs are taken from (71,72) for PC. Error bars are no greater than the size of the symbols, except for open circles. Solid lines connect values simulated with CHARMM36 (*solid squares*), and dashed lines those with the force field of Berger et al. (*solid circles*), but have no other significance. All samples are in water without ions, except for S_{PO_4} where 50 mM Tris, 1 mM EDTA pH 7.4 (82), or 20 mM NaCl, 30 mM HEPES, 5 mM EDTA pH 7.0 (80,81) buffers are used.

improvements in agreement with NMR order parameters are unlikely to compromise agreement with area/molecule and molecular thicknesses. But whether this extends from dimensional properties to the elastic and thermodynamic properties of lipid bilayers is less certain.

SUPPORTING MATERIAL

One figure and one table are available at http://www.biophysj.org/biophysj/supplemental/S0006-3495(18)30246-7.

AUTHOR CONTRIBUTIONS

D.M. and H.K. designed research. W.P. performed research. D.M. wrote paper together with the other authors.

ACKNOWLEDGMENTS

D.M. thanks the Hans Christian Andersen Foundation (University of Southern Denmark) and Christian Griesinger and the Department of NMR-Based Structural Biology (Max-Planck-Institut) for financial assistance.

REFERENCES

1. Hauser, H., I. Pascher, …, S. Sundell. 1981. Preferred conformation and molecular packing of phosphatidylethanolamine and phosphatidylcholine. *Biochim. Biophys. Acta.* 650:21–51.
2. Pascher, I., M. Lundmark, …, S. Sundell. 1992. Crystal structures of membrane lipids. *Biochim. Biophys. Acta.* 1113:339–373.
3. Pascher, I. 1996. The different conformations of the glycerol region of crystalline acylglycerols. *Curr. Opin. Struct. Biol.* 6:439–448.
4. Marsh, D. 2013. Handbook of Lipid Bilayers. CRC Press, Boca Raton, FL.
5. Marsh, D. 2003. Lipid-binding proteins: structure of the phospholipid ligands. *Protein Sci.* 12:2109–2117.
6. Marsh, D., and T. Páli. 2006. Lipid conformation in crystalline bilayers and in crystals of transmembrane proteins. *Chem. Phys. Lipids.* 141:48–65.
7. Marsh, D., and T. Páli. 2013. Orientation and conformation of lipids in crystals of transmembrane proteins. *Eur. Biophys. J.* 42:119–146.
8. Seelig, A., and J. Seelig. 1975. Bilayers of dipalmitoyl-3-*sn*-phosphatidylcholine. Conformational differences between the fatty acyl chains. *Biochim. Biophys. Acta.* 406:1–5.
9. Seelig, J., and J. L. Browning. 1978. General features of phospholipid conformation in membranes. *FEBS Lett.* 92:41–44.
10. Marsh, D., A. Watts, and I. C. P. Smith. 1983. Dynamic structure and phase behavior of dimyristoylphosphatidylethanolamine bilayers studied by deuterium nuclear magnetic resonance. *Biochemistry.* 22:3023–3026.
11. Seelig, J., H. U. Gally, and R. Wohlgemuth. 1977. Orientation and flexibility of the choline head group in phosphatidylcholine bilayers. *Biochim. Biophys. Acta.* 467:109–119.
12. Seelig, J., and H. U. Gally. 1976. Investigation of phosphatidylethanolamine bilayers by deuterium and phosphorus-31 nuclear magnetic resonance. *Biochemistry.* 15:5199–5204.
13. Hong, M., K. Schmidt-Rohr, and H. Zimmermann. 1996. Conformational constraints on the headgroup and *sn*-2 chain of bilayer DMPC from NMR dipolar couplings. *Biochemistry.* 35:8335–8341.
14. Schlenkrich, M., J. Brickmann, …, M. Karplus. 1996. An empirical potential energy function for phospholipids: criteria for parameter optimization and applications. *In* Biological Membranes: A Molecular Perspective from Computation and Experiment. K. M. Merz, Jr. and B. Roux, eds. Birkhäuser, pp. 31–81.
15. Klauda, J. B., R. M. Venable, …, R. W. Pastor. 2008. Considerations for lipid force field development. *In* Current Topics in Membranes: Computational Modeling of Membrane Bilayers. S. E. Feller, ed. Elsevier, pp. 1–48.
16. Sapay, N., and D. P. Tielemann. 2008. Molecular dynamics simulation of lipid-protein interactions. *In* Current Topics in Membranes: Computational Modeling of Membrane Bilayers. S. E. Feller, ed. Elsevier, pp. 111–130.
17. Pastor, R. W., and A. D. Mackerell, Jr. 2011. Development of the CHARMM force field for lipids. *J. Phys. Chem. Lett.* 2:1526–1532.

18. Venable, R. M., F. L. H. Brown, and R. W. Pastor. 2015. Mechanical properties of lipid bilayers from molecular dynamics simulation. *Chem. Phys. Lipids.* 192:60–74.
19. Egberts, E., S.-J. Marrink, and H. J. C. Berendsen. 1994. Molecular dynamics simulation of a phospholipid membrane. *Eur. Biophys. J.* 22:423–436.
20. Berger, O., O. Edholm, and F. Jähnig. 1997. Molecular dynamics simulations of a fluid bilayer of dipalmitoylphosphatidylcholine at full hydration, constant pressure, and constant temperature. *Biophys. J.* 72:2002–2013.
21. Klauda, J. B., R. M. Venable, …, R. W. Pastor. 2010. Update of the CHARMM all-atom additive force field for lipids: validation on six lipid types. *J. Phys. Chem. B.* 114:7830–7843.
22. Marsh, D. 1996. Lateral pressure in membranes. *Biochim. Biophys. Acta.* 1286:183–223.
23. Marsh, D. 1997. Renormalization of the tension and area expansion modulus in fluid membranes. *Biophys. J.* 73:865–869.
24. Chiu, S. W., M. Clark, …, E. Jakobsson. 1995. Incorporation of surface tension into molecular dynamics simulation of an interface: a fluid phase lipid bilayer membrane. *Biophys. J.* 69:1230–1245.
25. Khandelia, H., S. Witzke, and O. G. Mouritsen. 2010. Interaction of salicylate and a terpenoid plant extract with model membranes: reconciling experiments and simulations. *Biophys. J.* 99:3887–3894.
26. Venable, R. M., Y. Luo, …, R. W. Pastor. 2013. Simulations of anionic lipid membranes: development of interaction-specific ion parameters and validation using NMR data. *J. Phys. Chem. B.* 117:10183–10192.
27. Catte, A., M. Girych, …, S. Vilov. 2016. Molecular electrometer and binding of cations to phospholipid bilayers. *Phys. Chem. Chem. Phys.* 18:32560–32569.
28. Poger, D., B. Caron, and A. E. Mark. 2016. Validating lipid force fields against experimental data: progress, challenges and perspectives. *Biochim. Biophys. Acta.* 1858:1556–1565.
29. Botan, A., F. Favela-Rosales, …, J. Tynkkynen. 2015. Toward atomistic resolution structure of phosphatidylcholine headgroup and glycerol backbone at different ambient conditions. *J. Phys. Chem. B.* 119:15075–15088.
30. Sonne, J., M. O. Jensen, …, G. H. Peters. 2007. Reparameterization of all-atom dipalmitoylphosphatidylcholine lipid parameters enables simulation of fluid bilayers at zero tension. *Biophys. J.* 92:4157–4167.
31. Klauda, J. B., N. Kucerka, …, J. F. Nagle. 2006. Simulation-based methods for interpreting x-ray data from lipid bilayers. *Biophys. J.* 90:2796–2807.
32. Galindo-Murillo, R., J. C. Robertson, …, T. E. Cheatham, III. 2016. Assessing the current state of AMBER force field modifications for DNA. *J. Chem. Theory Comput.* 12:4114–4127.
33. Lindorff-Larsen, K., P. Maragakis, …, D. E. Shaw. 2012. Systematic validation of protein force fields against experimental data. *PLoS One.* 7:e32131.
34. Piana, S., K. Lindorff-Larsen, and D. E. Shaw. 2011. How robust are protein folding simulations with respect to force field parameterization? *Biophys. J.* 100:L47–L49.
35. Lange, O. F., D. van der Spoel, and B. L. de Groot. 2010. Scrutinizing molecular mechanics force fields on the submicrosecond timescale with NMR data. *Biophys. J.* 99:647–655.
36. Huang, J., S. Rauscher, …, A. D. MacKerell, Jr. 2017. CHARMM36m: an improved force field for folded and intrinsically disordered proteins. *Nat. Methods.* 14:71–73.
37. Sezer, D., J. H. Freed, and B. Roux. 2009. Multifrequency electron spin resonance spectra of a spin-labeled protein calculated from molecular dynamics simulations. *J. Am. Chem. Soc.* 131:2597–2605.
38. Kuprusevicius, E., G. White, and V. S. Oganesyan. 2011. Prediction of nitroxide spin label EPR spectra from MD trajectories: application to myoglobin. *Faraday Discuss.* 148:283–298.
39. Budil, D. E., K. L. Sale, …, P. G. Fajer. 2006. Calculating slow-motional electron paramagnetic resonance spectra from molecular dynamics using a diffusion operator approach. *J. Phys. Chem. A.* 110:3703–3713.
40. Kassem, M. M., Y. Wang, …, K. Lindorff-Larsen. 2016. Structure of the bacterial cytoskeleton protein bactofilin by NMR chemical shifts and sequence variation. *Biophys. J.* 110:2342–2348.
41. Rauscher, S., V. Gapsys, …, H. Grubmüller. 2015. Structural ensembles of intrinsically disordered proteins depend strongly on force field: a comparison to experiment. *J. Chem. Theory Comput.* 11:5513–5524.
42. Beauchamp, K. A., Y.-S. Lin, …, V. S. Pande. 2012. Are protein force fields getting better? A systematic benchmark on 524 diverse NMR measurements. *J. Chem. Theory Comput.* 8:1409–1414.
43. Best, R. B., H. Hofmann, …, B. Schuler. 2015. Quantitative interpretation of FRET experiments via molecular simulation: force field and validation. *Biophys. J.* 108:2721–2731.
44. Reif, M. M., and C. Oostenbrink. 2014. Molecular dynamics simulation of configurational ensembles compatible with experimental FRET efficiency data through a restraint on instantaneous FRET efficiencies. *J. Comput. Chem.* 35:2319–2332.
45. Hoefling, M., N. Lima, …, H. Grubmüller. 2011. Structural heterogeneity and quantitative FRET efficiency distributions of polyprolines through a hybrid atomistic simulation and Monte Carlo approach. *PLoS One.* 6:e19791.
46. Sundaralingam, M. 1972. Discussion paper: molecular structures and conformations of the phospholipids and sphingomyelins. *Ann. N. Y. Acad. Sci.* 195:324–355.
47. IUPAC Commission on Nomenclature of Organic Chemistry. 1976. Rules for the nomenclature of organic chemistry. Section E: stereochemistry. *Pure Appl. Chem.* 45:11–30.
48. IUPAC-IUB Commission on Biochemical Nomenclature (CBN). 1970. Nomenclature of lipids. Amendments 1968. *Eur. J. Biochem.* 12:1–2.
49. Klyne, W., and V. Prelog. 1960. Description of steric relationships across single bonds. *Experientia.* 16:521–523.
50. Berendsen, H. J. C., D. van der Spoel, and R. van Drunen. 1995. GROMACS: a message-passing parallel molecular dynamics implementation. *Comput. Phys. Commun.* 91:43–56.
51. Van Der Spoel, D., E. Lindahl, …, H. J. C. Berendsen. 2005. GROMACS: fast, flexible, and free. *J. Comput. Chem.* 26:1701–1718.
52. Hess, B., C. Kutzner, …, E. Lindahl. 2008. GROMACS 4: algorithms for highly efficient, load-balanced and scalable molecular simulation. *J. Chem. Theory Comput.* 4:435–447.
53. MacKerell, A. D., D. Bashford, …, M. Karplus. 1998. All-atom empirical potential for molecular modeling and dynamics studies of proteins. *J. Phys. Chem. B.* 102:3586–3616.
54. Berendsen, H. J. C., J. P. M. Postma, …, J. Hermans. 1981. Interaction models for water in relation to protein hydration. *In* Intermolecular Forces (Jerusalem Symposia). B. Pullman, ed. Springer, pp. 331–342.
55. Hess, B., H. Bekker, …, J. G. E. M. Fraaije. 1997. LINCS: a linear constraint solver for molecular simulations. *J. Comput. Chem.* 18:1463–1472.
56. Kopec, W., and H. Khandelia. 2014. Reinforcing the membrane-mediated mechanism of action of the anti-tuberculosis candidate drug thioridazine with molecular simulations. *J. Comput. Aided Mol. Des.* 28:123–134.
57. Darden, T., D. York, and N. C. Pedersen. 1993. Particle mesh Ewald: an N-log(N) method for Ewald sums in large systems. *J. Chem. Phys.* 98:10089–10092.
58. Essmann, U., L. Perera, …, L. G. Pedersen. 1995. A smooth particle mesh Ewald method. *J. Chem. Phys.* 103:8577–8593.
59. Berendsen, H. J. C., J. P. M. Postma, …, J. R. Haak. 1984. Molecular dynamics with coupling to an external bath. *J. Chem. Phys.* 81:3684–3690.
60. Hoover, W. G. 1985. Canonical dynamics: equilibrium phase-space distributions. *Phys. Rev. A Gen. Phys.* 31:1695–1697.

61. Parrinello, M., and A. Rahman. 1981. Polymorphic transitions in single-crystals - a new molecular-dynamics method. *J. Appl. Phys.* 52:7182–7190.

62. Schorn, K., and D. Marsh. 1996. Dynamic chain conformations in dimyristoyl glycerol-dimyristoyl phosphatidylcholine mixtures. ^{2}H-NMR studies. *Biophys. J.* 71:3320–3329.

63. Gally, H. U., W. Niederberger, and J. Seelig. 1975. Conformation and motion of the choline head group in bilayers of dipalmitoyl-3-*sn*-phosphatidylcholine. *Biochemistry.* 14:3647–3652.

64. Pearson, R. H., and I. Pascher. 1979. The molecular structure of lecithin dihydrate. *Nature.* 281:499–501.

65. Siminovitch, D. J., M. Rance, and K. R. Jeffrey. 1980. The use of wide-line ^{14}N nitrogen NMR as a probe in model membranes. *FEBS Lett.* 112:79–82.

66. Seelig, J. 1978. ^{31}P nuclear magnetic resonance and the head group structure of phospholipids in membranes. *Biochim. Biophys. Acta.* 515:105–140.

67. Dufourc, E. J., C. Mayer, …, G. Kothe. 1992. Dynamics of phosphate head groups in biomembranes. Comprehensive analysis using phosphorus-31 nuclear magnetic resonance lineshape and relaxation time measurements. *Biophys. J.* 61:42–57.

68. Griffin, R. G., L. Powers, and P. S. Pershan. 1978. Head-group conformation in phospholipids: a phosphorus-31 nuclear magnetic resonance study of oriented monodomain dipalmitoylphosphatidylcholine bilayers. *Biochemistry.* 17:2718–2722.

69. Marsh, D., and M. J. Swamy. 2000. Derivatised lipids in membranes. Physico-chemical aspects of *N*-biotinyl phosphatidylethanolamines, *N*-acyl phosphatidylethanolamines and *N*-acyl ethanolamines. *Chem. Phys. Lipids.* 105:43–69.

70. Santos, J. S., D.-K. Lee, and A. Ramamoorthy. 2004. Effects of antidepressants on the conformation of phospholipid headgroups studied by solid-state NMR. *Magn. Reson. Chem.* 42:105–114.

71. Gross, J. D., D. E. Warschawski, and R. G. Griffin. 1997. Dipolar recoupling in MAS NMR: a probe for segmental order in lipid bilayers. *J. Am. Chem. Soc.* 119:796–802.

72. Hong, M., K. Schmidt-Rohr, and D. Nanz. 1995. Study of phospholipid structure by ^{1}H, ^{13}C, and ^{31}P dipolar couplings from two-dimensional NMR. *Biophys. J.* 69:1939–1950.

73. Gorenstein, D. G., and D. Kar. 1977. Effect of bond angle distortion on torsional potentials. Ab initio and CNDO/2 calculations on dimethoxymethane and dimethyl phosphate. *J. Am. Chem. Soc.* 99:672–677.

74. Akutsu, H. 1981. Direct determination by Raman scattering of the conformation of the choline group in phospholipid bilayers. *Biochemistry.* 20:7359–7366.

75. Abe, A., and J. E. Mark. 1976. Conformational energies and the random-coil dimensions and dipole-moments of the polyoxides $CH_3O[(CH_2)_yO]_xCH_3$. *J. Am. Chem. Soc.* 98:6468–6476.

76. Flory, P. J. 1969. Statistical Mechanics of Chain Molecules. Wiley, London or New York.

77. Li, S., H. N. Lin, …, C. Huang. 1994. Identification and characterization of kink motifs in 1-palmitoyl-2-oleoyl-phosphatidylcholines: a molecular mechanics study. *Biophys. J.* 66:2005–2018.

78. Akutsu, H., and T. Nagamori. 1991. Conformational analysis of the polar head group in phosphatidylcholine bilayers: a structural change induced by cations. *Biochemistry.* 30:4510–4516.

79. Skarjune, R., and E. Oldfield. 1979. Physical studies of cell surface and cell membrane structure. Determination of phospholipid head group organization by deuterium and phosphorus nuclear magnetic resonance spectroscopy. *Biochemistry.* 18:5903–5909.

80. Zhang, L., L. Liu, …, C. Dabney-Smith. 2014. Investigating the interaction between peptides of the amphipathic helix of Hcf106 and the phospholipid bilayer by solid-state NMR spectroscopy. *Biochim. Biophys. Acta.* 1838:413–418.

81. Lu, J. X., J. Blazyk, and G. A. Lorigan. 2006. Exploring membrane selectivity of the antimicrobial peptide KIGAKI using solid-state NMR spectroscopy. *Biochim. Biophys. Acta.* 1758:1303–1313.

82. Tamm, L., and J. Seelig. 1983. Lipid solvation of cytochrome *c* oxidase. Deuterium, nitrogen-14, and phosphorus-31 nuclear magnetic resonance studies on the phosphocholine head group and on cis-unsaturated fatty acyl chains. *Biochemistry.* 22:1474–1483.

83. Ollila, O. H. S., and G. Pabst. 2016. Atomistic resolution structure and dynamics of lipid bilayers in simulations and experiments. *Biochim. Biophys. Acta.* 1858:2512–2528.

84. Semchyschyn, D. J., and P. M. Macdonald. 2004. Conformational response of the phosphatidylcholine headgroup to bilayer surface charge: torsion angle constraints from dipolar and quadrupolar couplings in bicelles. *Magn. Reson. Chem.* 42:89–104.

85. Ferreira, T. M., F. Coreta-Gomes, …, D. Topgaard. 2013. Cholesterol and POPC segmental order parameters in lipid membranes: solid state ^{1}H-^{13}C NMR and MD simulation studies. *Phys. Chem. Chem. Phys.* 15:1976–1989.

86. Khandelia, H., and O. G. Mouritsen. 2009. Lipid gymnastics: evidence of complete acyl chain reversal in oxidized phospholipids from molecular simulations. *Biophys. J.* 96:2734–2743.

87. McDaniel, R. V., A. McLaughlin, …, S. McLaughlin. 1984. Bilayer membranes containing the ganglioside GM1: models for electrostatic potentials adjacent to biological membranes. *Biochemistry.* 23:4618–4624.

88. Winiski, A. P., A. C. McLaughlin, …, S. McLaughlin. 1986. An experimental test of the discreteness-of-charge effect in positive and negative lipid bilayers. *Biochemistry.* 25:8206–8214.

89. Tatulian, S. A. 1987. Binding of alkaline-earth metal cations and some anions to phosphatidylcholine liposomes. *Eur. J. Biochem.* 170:413–420.

90. Macdonald, P. M., and J. Seelig. 1987. Calcium binding to mixed phosphatidylglycerol-phosphatidylcholine bilayers as studied by deuterium nuclear magnetic resonance. *Biochemistry.* 26:1231–1240.

91. Cevc, G., and D. Marsh. 1987. Phospholipid Bilayers. Physical Principles and Models. Wiley-Interscience, New York.

92. Marsh, D. 1974. Statistical mechanics of the fluidity of phospholipid bilayers and membranes. *J. Membr. Biol.* 18:145–162.

93. Feller, S. E., and A. D. MacKerell, Jr. 2000. An improved empirical potential energy function for molecular simulations of phospholipids. *J. Phys. Chem. B.* 104:7510–7515.

94. Moser, M., D. Marsh, …, G. Kothe. 1989. Chain configuration and flexibility gradient in phospholipid membranes. Comparison between spin-label electron spin resonance and deuteron nuclear magnetic resonance, and identification of new conformations. *Biophys. J.* 55:111–123.

95. Mendelsohn, R., M. A. Davies, …, R. A. Dluhy. 1989. Quantitative determination of conformational disorder in the acyl chains of phospholipid bilayers by infrared spectroscopy. *Biochemistry.* 28:8934–8939.

96. Casal, H. L., and R. N. McElhaney. 1990. Quantitative determination of hydrocarbon chain conformational order in bilayers of saturated phosphatidylcholines of various chain lengths by Fourier transform infrared spectroscopy. *Biochemistry.* 29:5423–5427.

97. Gally, H. U., G. Pluschke, …, J. Seelig. 1981. Structure of *Escherichia coli* membranes. Glycerol auxotrophs as a tool for the analysis of the phospholipid head-group region by deuterium magentic resonance. *Biochemistry.* 20:1826–1831.

98. Bechinger, B., and J. Seelig. 1991. Conformational changes of the phosphatidylcholine headgroup due to membrane dehydration. A ^{2}H-NMR study. *Chem. Phys. Lipids.* 58:1–5.

99. Stockton, G. W., C. F. Polnaszek, …, I. C. P. Smith. 1976. Molecular motion and order in single-bilayer vesicles and multilamellar dispersions of egg lecithin and lecithin-cholesterol mixtures. A deuterium nuclear magnetic resonance study of specifically labeled lipids. *Biochemistry.* 15:954–966.

Biophysical Journal, Volume *114*

Supplemental Information

Lipid Configurations from Molecular Dynamics Simulations

Weria Pezeshkian, Himanshu Khandelia, and Derek Marsh

Supporting Material

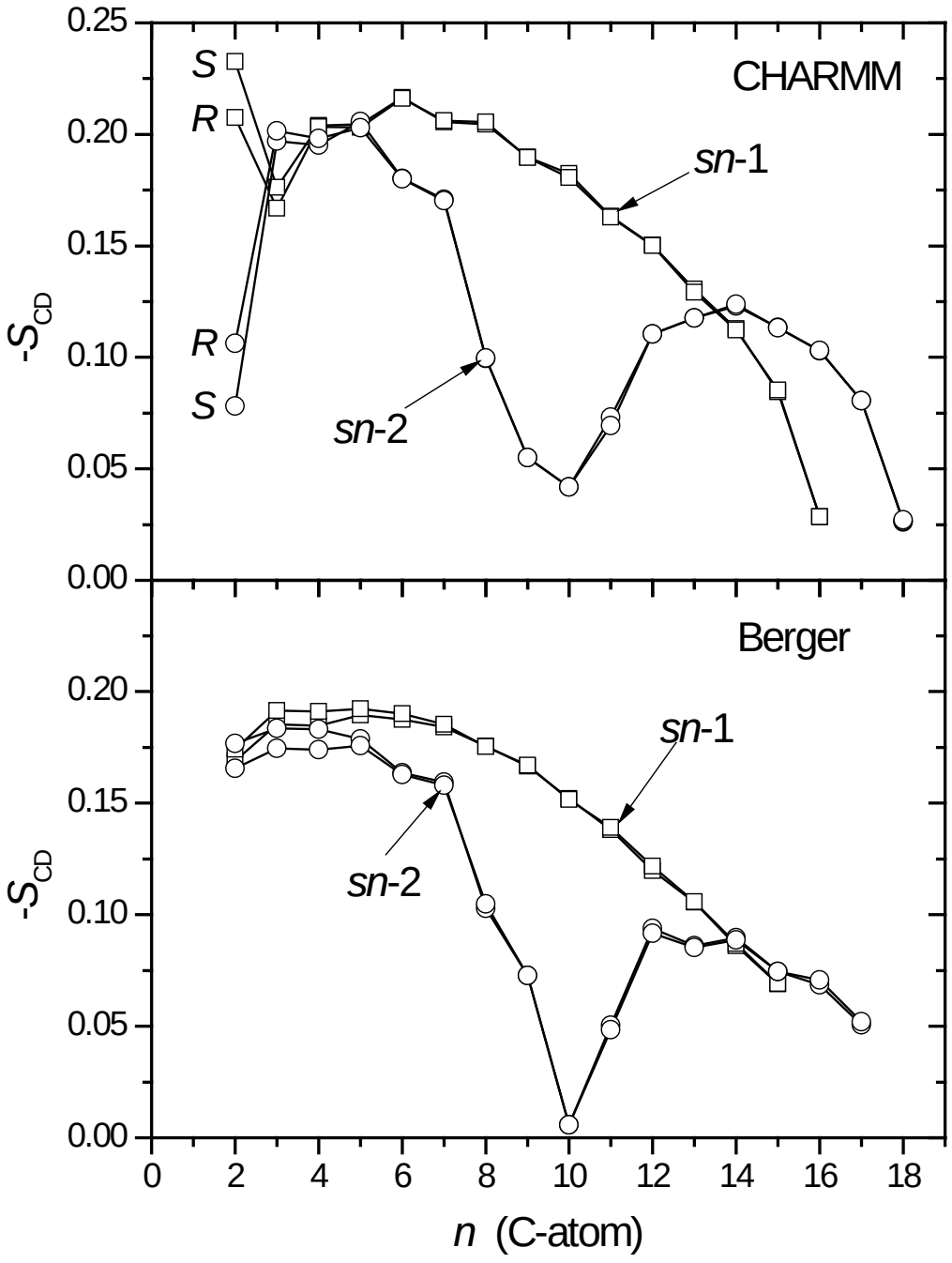

Fig. S.1 C–D order parameters of the *sn*-1 (squares) and *sn*-2 (circles) chains of POPC. MD simulations using the CHARMM36 (top panel) and Berger et al. (bottom panel) force fields. Prochirality (*R*,*S*) of the H-atoms on C2 is indicated.

Table S.1 Comparison of partial atomic charges for united atoms of the Berger et al. force field.

atom	CHARMM[a]	Berger et al.[b]	atom	CHARMM[a]	Berger et al.[b]
N	-0.60	-0.50	C2	0.26	0.30
C33,C34,C35	0.40	0.40	O21	-0.49	-0.70
C32	0.40	0.30	C21	0.90	0.70
C31	0.10	0.40	O22	-0.63	-0.70
P	1.50	1.70	C22	-0.04	0.00
O33,O34	-0.78	-0.80	C3	0.26	0.50
O32	-0.57	-0.80	O31	-0.49	-0.70
O31	-0.57	-0.70	C31	0.90	0.80
C3	0.10	0.40	O32	-0.63	-0.60
			C32	-0.04	0.00

[a] Net atomic charge in CHARMM36 (21) corresponding to the united atoms used for the force field of Berger et al. (20).
[b] Taken from quantum chemical calculations of Chiu et al. (24).